Available online at www.sciencedirect.com

ScienceDirect

Energy Procedia 114 (2017) 5229 – 5240

Energy Procedia

13th International Conference on Greenhouse Gas Control Technologies, GHGT-13, 14-18 November 2016, Lausanne, Switzerland

Unusual corrosion behavior of 1.4542 exposed a laboratory saline aquifer water CCS-environment

Anja Pfennig[a]*, Helmut Wolthusen[a], and Axel Kranzmann[b]*

[a] *HTW University of Applied Sciences Berlin, Wilhelminenhofstraße 75 A, Gebäude C, 12459 Berlin, Germany*
[b] *BAM Federal Institute of Materials Research and Testing, Unter den Eichen 87, 12205 Berlin, Germany*

Abstract

Differently heat treated coupons of 1.4542 were kept at T=60 °C and ambient pressure as well as p=100 bar for 700 h - 8000 h in an a) water saturated supercritical CO2 and b) CO2-saturated synthetic aquifer environment similar to on-shore CCS-sites in the Northern German Basin. Surface corrosion layers are homogeneous but unusually discontinuously ellipsoidal. After 8000 h at 100 bar maximum corrosion rate in the liquid phase is approximately 0.014 mm/year, with normalizing providing best corrosion resistance and approximately 0.003 mm/year in the supercritical phase where hardening+tempering at 670 °C leads to lowest corrosion rates.

Peer-review under responsibility of the organizing committee of GHGT-13.

Keywords: steel; supercritical CO_2; pipeline; corrosion; CCS; CO_2-storage

1. Introduction

Carbon capture and storage (CCS) is considered to mitigate global warming by reducing the emission of the greenhouse gas CO_2. The CCS procedure includes 3 phases: 1st the capture of CO_2 and emission gasses directly from combustion processes at the source (e.g. coal power plants) and its compression, 2nd the transmission through pipelines and 3rd the injection into adequate geological formations [1,2]. For storage CO_2 is expected to be pressurized to a supercritical (or liquid) state [3,4]. During enhanced oil recovery compressed technically clean CO2

* Corresponding author. Tel.: +49 30 8104 3119; fax: +49 30 8104 1517.
E-mail address: anja.pfennig@htw-berlin.de.

Peer-review under responsibility of the organizing committee of GHGT-13.
doi:10.1016/j.egypro.2017.03.1679

with very low concentration of impurities is transmitted through pipelines [3]. Still, there is very little knowledge on the corrosion behavior of steels in supercritical CO_2 that occurs in water saturated supercritical CO_2, but not in pure supercritical CO_2 [5]. During the injection of CO_2 into deep geological saline aquifer reservoirs as found in the Northern German Basin [6-8], the CO_2 is dissolved in the brine to build a corrosive environment. This may easily cause failure of pipe steels [9-11]. Due to the anodic iron dissolution of the pipe steel a $FeCO_3$ corrosion layer (siderite) grows on the alloy surface [12]. Internal corrosion will depend largely upon the source of the injected gas, its composition and the presence of water and dissolved salts [9,10]. During intermissions of the injection process corrosion of the injection pipe in CO2-rich aquifer water may be a possibility in case of the formation of phase boundaries when the aquifer water may flow back into the injection pipe [13,14].

1.4542 stainless steel (AISI 630, X5CrNiCuNb16-4) is a precipitation hardening martensitic stainless steel with about 3% copper with small size copper distributed in the matrix ensuring the precipitation hardening mechanism [15]. Islands of niobium and copper carbides are embedded within the microstructure of 1.4542 characterized by layers of the martensitic matrix of bcc-structure [16]. This increases the strength of the material and ensures excellent mechanical properties as well as good corrosion resistance. But, 1.4542 is known to be susceptible towards stress corrosion cracking (SCC) and less corrosion resistant compared to its solution treated state with lower strength.

The influence of heat treatment, that is: temperature and time of austenitizing, cooling rate as well as temperature and time of annealing, has been shown by various authors and was summarized by Pfennig et al. [17]: Retained austenite as a microstructure component resulting from the heat treatments applied has a beneficial effect on the pitting corrosion resistance of 13%-chromium steels (13CrNiMo) [18]. A higher Ni and Cr content in the heat treated steels improve the corrosion resistance [18-21]. In general, raising the annealing temperature lowers the pitting potential of lean duplex stainless steels [20,22-23]. The increased corrosion resistance of martensitic stainless steels with 13% Cr at higher austenitizing temperature (980-1050 °C) is related to the dissolution of carbides [24-26]. The precipitation of Cr-rich $M_{23}C_6$ and M_7C_3 carbides reduced the resistance of passive film and pitting corrosion [23] and has high impact on mechanical properties due to secondary hardening [24]. The influence of heat treatment on microstructure and mechanical properties is well known [23,26,27]. However for C-Mn (carbon) steels offering excellent mechanical strength the martensitic microstructure has the highest corrosion rate in a H_2S-containing NaCl solution up to two orders of magnitude higher than ferritic or ferritic-bainitic microstructures due to the fact that martensitic grain boundaries are more reactive [27].

The dependence on environmental factors, e.g. the composition of surrounding media and alloy, temperature, CO_2 partial pressure, flow conditions, contaminations and formation of protective scales is shown by various authors [12,28,29]. 60 °C is well known for severe corrosion processes [11, 13,14,30-35]. This study introduces the unusual corrosion behavior of differently heat treated coupons of 1.4542 prior to exposure to a laboratory CCS environment simulating the hydrostatic pressure within the storage site and the critical temperature region of 60 °C.

2. Material and Methods

Exposure tests were carried out using samples made of thermally treated specimen of 1.4542 (X5CrNiCuNb16-4, AISI 630) with 8 mm thickness and 20 mm width and 50 mm length. A hole of 3.9 mm diameter was used for sample positioning (Table 1).

Table 1: Chemical composition of 1.4542 (X5CrNiCuNb16-4, AISI 630), no Co detected.

Elements	C	Si	Mn	P	S	Cr	Mo	Ni	Cu	Nb	Fe
acc standard [a]	≤ 0.07	≤ 0.70	≤ 1.50	≤ 0.04	≤ 0.015	15.0 - 17.0	≤ 0.60	3.00 – 5.00	3.00 – 5.00	0.20 – 0.45	rest
analysed [b]	0.03	0.42	0.68	0.018	0.002	15.75	0.11	4.54	3.00	0.242	75.00

a) elements as specified according to **DIN EN 10088-3 in %**
b) spark emission spectrometry

Heat treatment prior to exposure was done following routine protocols according to the 3 steel qualities (Table 2).

Table 2: Heat treatment of 1.4542 prior to exposure to CO_2-saturated aquifer at 100 bar.

heat treatment	temperature °C / °C	dwell time min	cooling medium
normalizing	850	30	oil
hardening	1040	30	oil
hardening + tempering 1, 600 °C	1040 / 550	30	oil
hardening + tempering 2, 670 °C	1040 / 650	30	oil
hardening + tempering 3, 700 °C	1040 / 755	30	oil

The microstructure reveals martensite with different needle shaped sizes and increasing percentage of precipitation with increasing tempering temperature (Fig. 1).

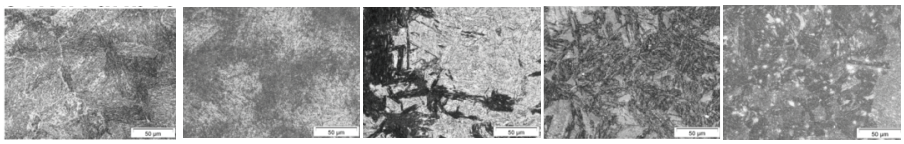

microstructure					
heat treatment	normalizing	hardening	hardening and tempering at 550 °C	hardening and tempering at 650 °C	hardening and tempering at 755 °C

Fig. 1: Microstructure of 1.4542 coupons prior to exposure.

The surfaces were activated by grinding with SiC-Paper down to 120 µm under water. Samples of each base metal were positioned within the vapour phase (1 bar), the supercritical phase (100 bar) and within the liquid phase. The brine (as known to be similar to the Stuttgart Aquifer [6 Ca^{2+}: 1760 mg/L, K^{2+}: 430 mg/L, Mg^{2+}: 1270 mg/L, Na^{2+}: 90,100 mg/L, Cl-: 143,300 mg/L, SO_4^{2-}: 3600 mg/L, HCO_3^-: 40 mg/L) was synthesized in a strictly orderly way to avoid precipitation of salts and carbonates (Fig. 2).

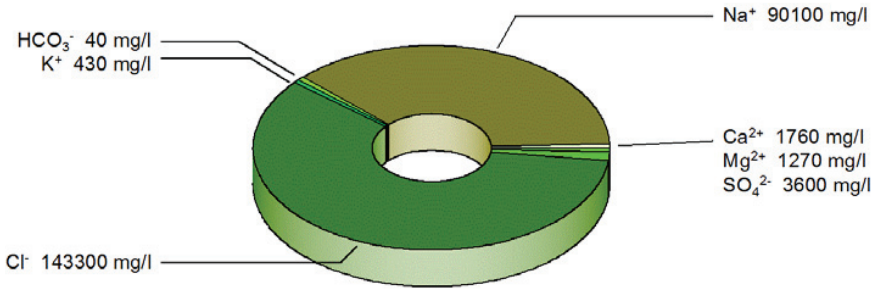

Fig. 2: Composition of laboratory saline aquifer brine according to [6].

The exposure of the samples between 700 h to 8000 h was disposed in a chamber kiln at 60 °C and ambient pressure and at 100 bar in an autoclave system (Figure 3) [17,36]. Flow control (3 NL/h) at ambient pressure was done by a capillary meter GDX600_man by QCAL Messtechnik GmbH, München [17].

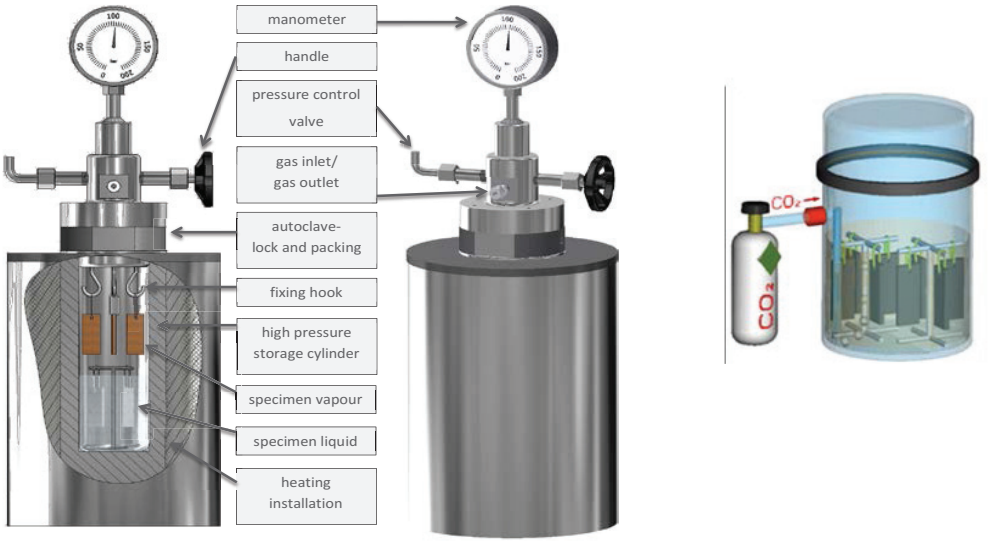

Fig. 3. Schematic set-up of laboratory in-situ experiment: left: autoclaves 100 bar/60 °C [36], right: ambient pressure/60 °C [17,37].

X-ray diffraction was carried out in a URD-6 (Seifert-FPM) with CoK_{α}-radiation with an automatic slit adjustment, step 0.03 and count 5 sec and AUTOQUAN ® by Seifert FPM was used for phase analysis. For gravimetric measurement descaling of the samples (60°C/700 h, 2000 h, 4000 h, 8000 h) was performed by exposure to 37% HCl for 24 hours and mass gain was analyzed according to DIN 50 905 part 1-4. To characterise surface corrosion SEM/EDX was performed using: Leo Gemini 1530 VP, acceleration voltage 15 kV. 3-D-images were realized to analyse pitting corrosion by the double optical system Microprof TTV by FRT. Non-descaled parts of the samples were embedded in a cold resin (Epoxicure, Buehler), cut and polished first with SiC-Paper from 180 µm to 1200 µm under water and then finished with diamond paste 6 µm, 3 µm and 1 µm. The measurement of the layer thicknesses and residual pipe wall thicknesses as well as microstructure analysis were performed via light and electron microscopy techniques using the semi-automatic analyzing program Analysis Docu ax-4 by Aquinto. A set of 100 linescans was measured taking 10 to 20 micrographs per parameter.

3. Results and Discussion

In general the CO_2 is injected in its supercritical phase. However, in the case of injection intermissions and reduced pressure in the injection pipe the water level may which may lead to the precipitation of the leopard shaped corrosion layer and formation of pits as stated.

Surface corrosion results in a discontinuous layer structure that may be related to als “leopard” structure. This unusual corrosion formation is present in supercritical water saturated CO_2 even after short exposure times (700 h) (Fig. 3) and in CO_2-saturated brine after 4000 h of exposure [37]. Here ellipsoidal regions of the sample surfaces are not corroded visually or are protected by a passivating layer while others show surface corrosion behavior.

In general, the leopard shaped corrosion layer reveals siderite $FeCO_3$ and goethite a-FeOOH als precipitation phases. The pit formation is driven by the formation of carbonic acid and existence of HCO_3 [36,37]. Pits are covered with corrosion products, mainly siderite as the main phase, as found on the surface elsewhere. Note, that experiments at ambient pressure with excess oxygen in the open system can overestimate the pit corrosion predicted resulting from higher corrosion rates and greater pit penetration depths at ambient pressure than at 100 bar.

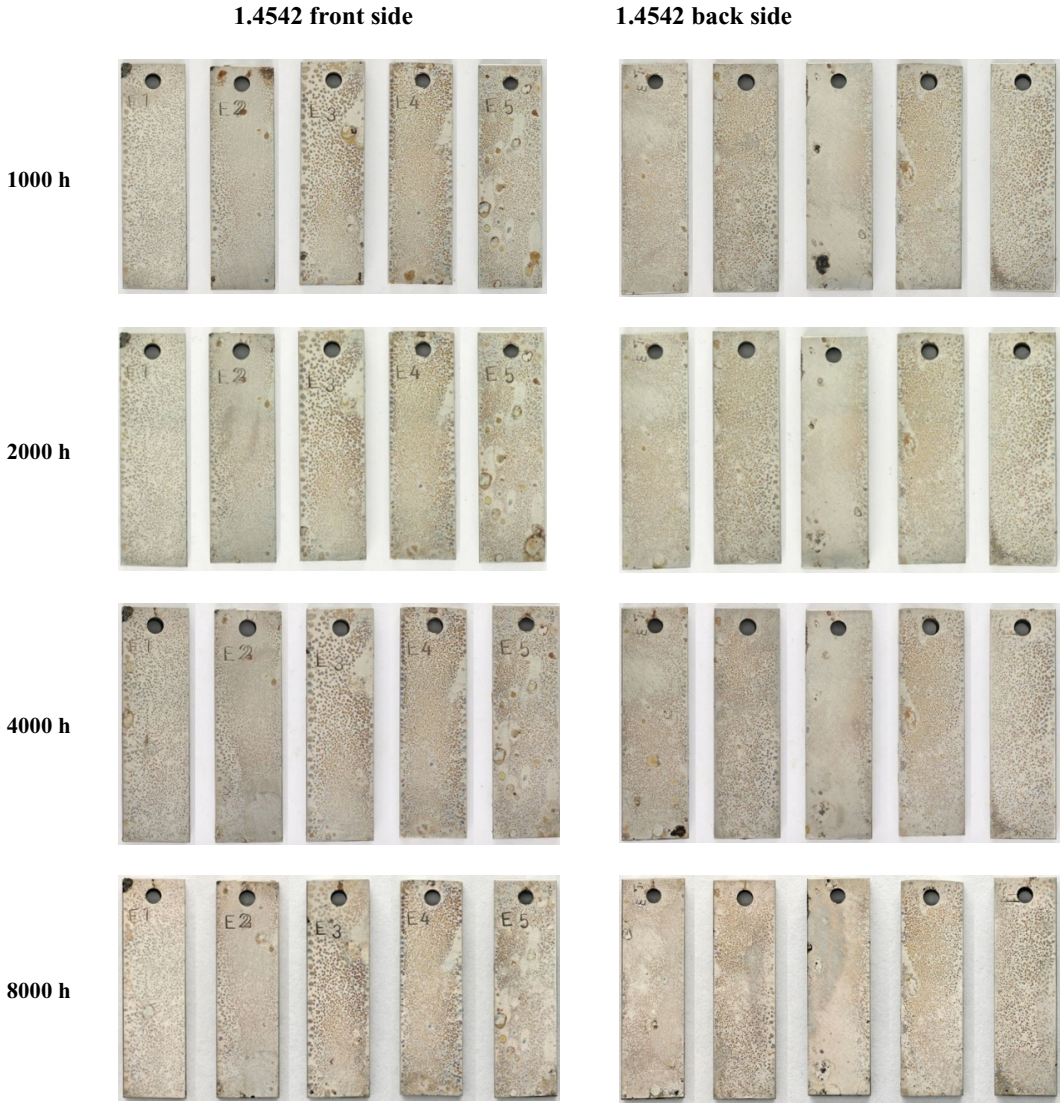

Fig. 4: Sample surfaces of differently heat treated X5CrNiCuNb16-4 after 1000 to 8000 hours of exposure to supercritical phase at 60 °C and 100 bar. Heat treatment from left to right: hardening at 1040 °C, hardening + tempering at 1040 °C + 550°C, 650 °C and 755 °C. Sample surfaces exposed to the liquid phase have been shown earlier [17].

3.1. Kinetics of surface corrosion

Fig. 5 shows the corrosion rates of 1.4542 in the liquid phase (right) and the supercritical phase (left) up to 8000 h. For reference also results obtained at ambient pressure are shown for samples exposed to the liquid phase. Both, samples exposed to water saturated supercritical CO_2 and CO_2-saturated brine do not reveal a distinct dependence on the heat treatment prior to exposure showing the same trends during over the entire exposure time. DIN 6601 allows corrosion rates of maximum 0.1 mm/year for pressure vessels. This criterion is met by all samples, even exposed to ambient pressure (maximum 0.025 mm/year).

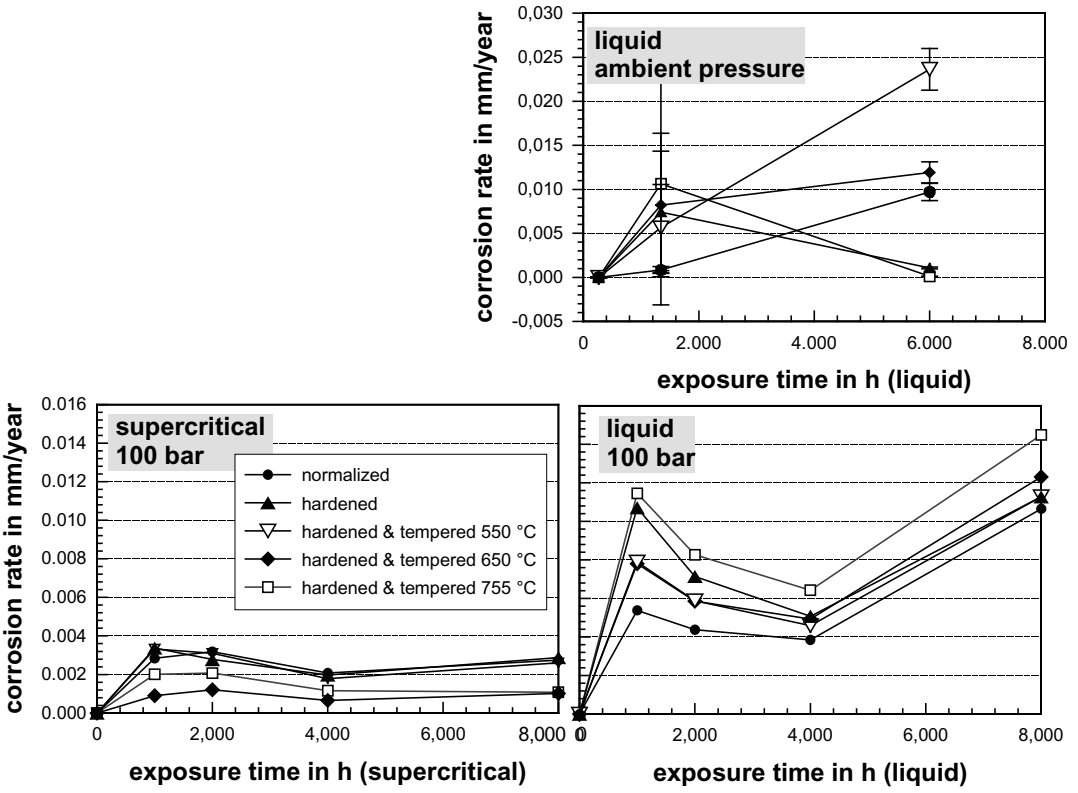

Fig. 5: Influence of heat treatment on the corrosion rate of 1.4542 in water saturated supercritical CO_2 (left) and CO_2 saturated saline aquifer water (right, taken from [36]) at 60 °C and 100 bar.

Maximum corrosion rate in the liquid phase is approximately 0.014 mm/year, after 8000 h and approximately 0.003 mm/year in the supercritical phase. In general, after 1000 h of exposure the corrosion rates decrease until approximately 4000 h indicating the precipitation of a passivating corrosion layer (incubation time). Longer exposure times lead to increasing surface corrosion rates after 4000 h of exposure due to a possible break-down of the passivating layer. The explicit increasing corrosion rates after long exposure to the CO_2-saturated saline aquifer environment may be due to increasing carbide precipitation. Carbides deplete the metal matrix surrounding the carbide of chromium and prohibit surface passivation. Consequently the base material decomposes after long exposure times and corrosion processes are accelerated.

In general samples exposed to water saturated supercritical CO_2 display the lowest corrosion rates from initial exposure to 8000 h due to a passivating nature of the corrosion scale formed at an early stage of the reaction: The cathodic reaction depending on the exchange of ionic species described in equation (1)

$$H_2CO_3 + H_2O \rightarrow H_3O^+ + HCO_3^- \quad (1)$$

is driven by the CO_2 partial pressure in the surrounding medium leading to an increasing H_2CO_3 concentration as in the CO_2 saturated liquid phase [10,31]. A higher partial pressure of the CO_2 in the water saturated supercritical CO_2 phase results in a more acidic and reactive environment. Then a passivating initial scale is formed quickly and

the corrosion process slows down. Another possible explanation is the lack of electrolytes in the supercritical CO_2 phase [37]. The passivating nature of the corrosion scale formed in supercritical CO_2 remains unchanged throughout the entire exposure time indicated by constant corrosion rates between 0.001 and 0.003 mm/year depending on the heat treatment. The thickness of the carbonate layer is sufficient enough to guarantee minimum mutual diffusion of ionic species into the base materials (CO_3^{2-} —and O^{2-} —species) and towards the outer surface (Fe-ions).

Corrosion rates obtained at ambient pressure are generally higher due to excess oxygen in the test system and accelerated corrosion reactions. This may also be related to an open capillary system within the corrosion layer suppressing fast mutual diffusion of ionic species at ambient pressure [33,37] relate this directly Under pressure, such a capillary system necessary for sufficient scale growth is not present.

Influence of heat treatment

The influence on heat treatment prior to exposure has been widely described [17,33,36,37]. Under supercritical CO_2 conditions a martensitic microstructure of hardened and tempered 1.4542 at low temperatures (650 °C) (< 0.001 mm/year) and under saline water normalized microstructure (ca. 0.004 mm/year) offer best corrosion resistance regarding surface corrosion (Fig. 5). At ambient pressure samples hardened and hardened and tempered at 755 °C show lowest corrosion rates, but here is very likely that the corrosion layer spalled from the metal surface leading to a rather high increase of the corrosion rate. Therefore, it is not possible to determine the influence of the heat treatment on the corrosion behaviour for 1.4542 at ambient pressure.

3.2. Kinetics of local corrosion

Fig. 6 shows the local of 1.4542 in the liquid phase (right) and the supercritical phase (left) up to 8000 h. For reference also results obtained at ambient pressure are shown for samples exposed to the liquid phase. Independent of the heat treatment 1.4542 developed pitting corrosion in both atmospheres, water saturated supercritical CO_2 (Fig. 6, left).and CO_2 saturated aquifer water (Fig. 6, right). Despite the alloying elements ensuring 1.4542 a good surface corrosion resistance this steel shows a rather high number of pits per m2 regardless of heat treatment prior to exposure. Opposite to the surface corrosion behavior the number of pits precipitated in the supercritical phase exceeds that precipitated in the liquid phase by an approximate factor of 10. The heat treatment hardening and tempering that showed minimum highest surface corrosion resistance now is the one to reveal greatest number of pits (Fig. 6, left). The number of pits after 8000 h are 50000 -260000 in the liquid phase and from 250000 to more than 1000000 in the supercritical phase. Pit depths measured after exposure at 100 bar and 60 °C are about 10-250 µm (Fig. 7). The lower number of pits at ambient pressure is due to the higher surface corrosion rate and rather large areas on the sample covered with siderite. Here pits have been consolidated and therefore counted as either single pit or measured as surface corrosion.

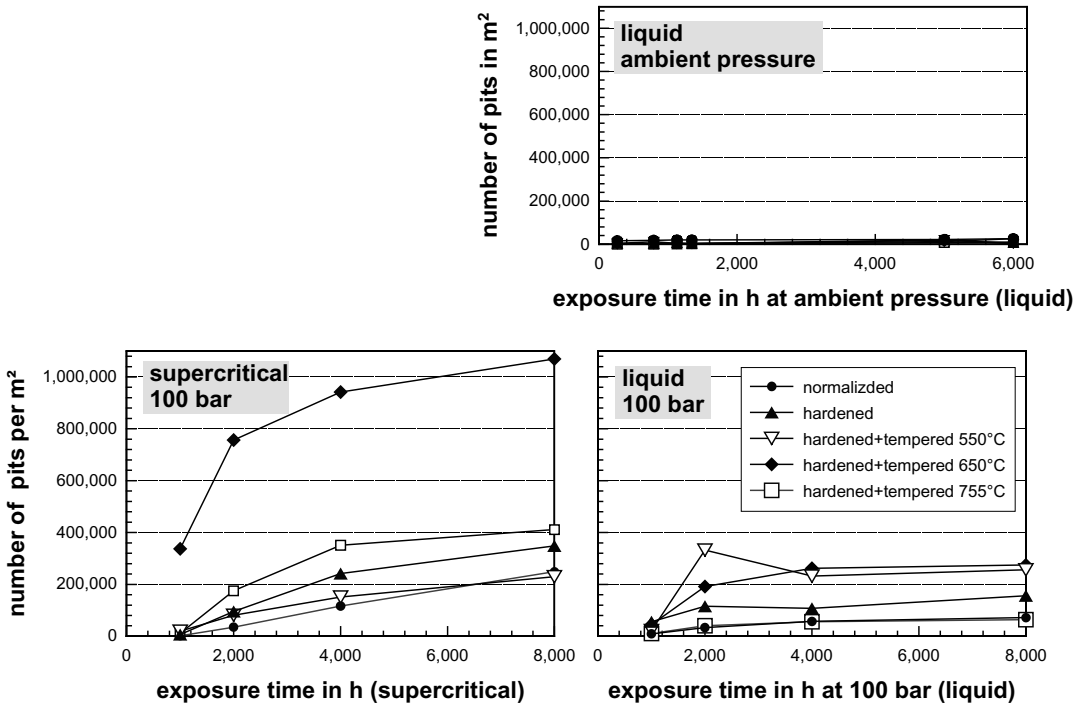

Fig. 6: Influence of heat treatment on the local corrosion of 1.4542 in water saturated supercritical CO_2 (left) and CO_2 saturated saline aquifer water (right, taken from [36]) at 60 °C and 100 bar.

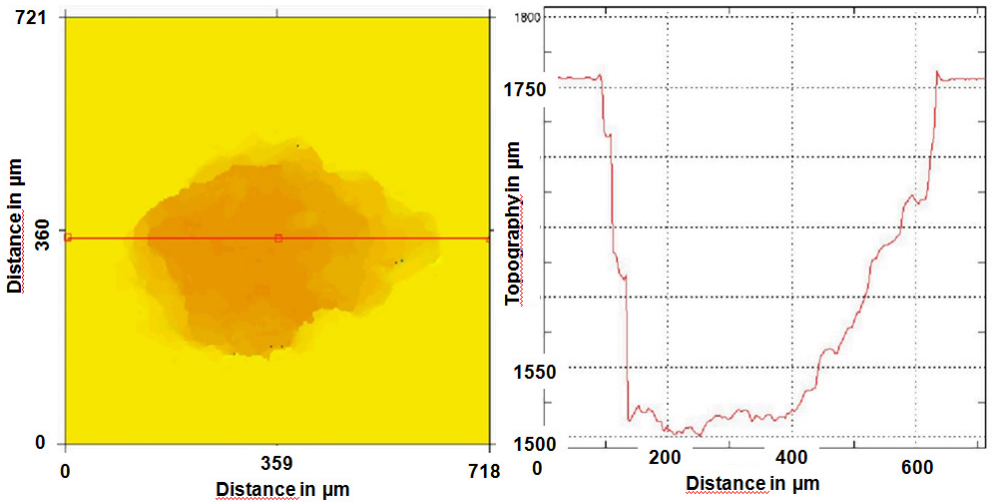

Fig. 7. Typical surface profiles with severe pit corrosion attack after 8000 hours of exposure at 60 °C and 100 bar of 1.4542 hardened prior to exposure.

3.3. Evaluation of corrosion behaviour

The surface corrosion layer on 1.4542 precipitates already after 1000 h of exposure at ambient pressure and more distinct at 100 bar increasing in thickness with exposure time (Fig. 5). These non-uniform corrosion layers differ in thickness but cover the entire sample surface. Specimens exposed to the water saturated supercritical CO2 and exposed for more than 4000 h to CO_2 saturated aquifer water form a discontinuous "leopard" shaped carbonate layer forming homogeneous ellipsoids. This results from a rather low pH in CO2-containing water forming carbonic acid and because the solubility of $FeCO_3$ is low [28] siderite forms in this unusual form as shown here. The ellipsoids show much higher oxygen content than the surrounding surface (Fig. 8) indicating an increased growth of the iron carbonate phase (siderite). The oxygen content decreases with increasing distance from the ellipsoids.

One possible explanation for this unusual behaviour forming homogeneous ellipsoids may be related to heterogeneous carbide distribution within the microstructure leading. Carbides are more susceptible to corrosion initiation [33] and therefore the passivation of the steel surface is locally destroyed.

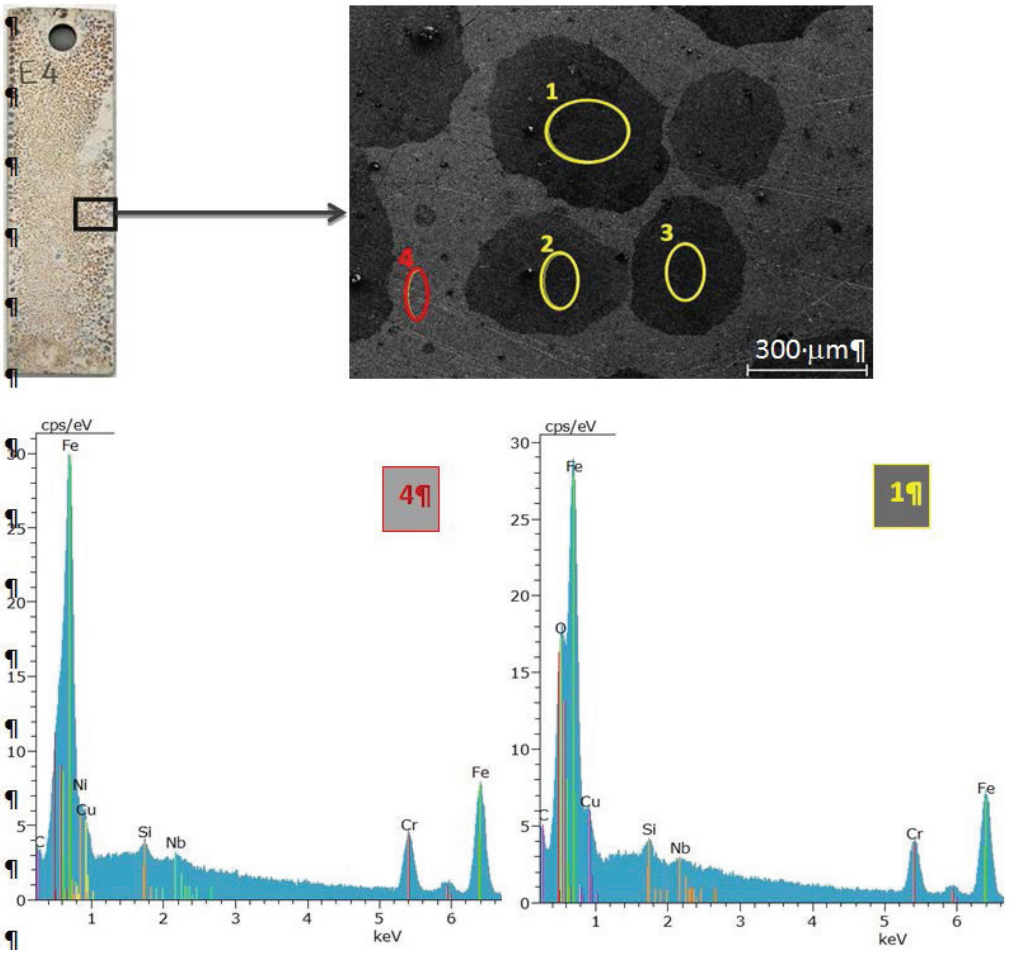

Fig. 8. SEM micrographs and element distribution of the ellipsoidal corrosion layer formed on 1.4542 hardened and tempered at 670 °C prior to exposure after 8000 hours of exposure at 60 °C and 100 bar to water saturated supercritical CO_2.

Another possible explanation is related to the dependence of water solubility on the pressure. The solubility of water decreases from 0 to 50 bar and then slightly increases again [31]. Increasing the temperature enhances the solubility of water. In water saturated supercritical CO_2 at 100bar and 60 °C the decreasing water solubility in the supercritical carbon dioxide leads to wetting of the metal surface by very thin and small water droplets. Because corrosion reactions are time dependent and time was too short to precipitate pits from the water droplets the typical "leopard" shaped corrosion layer is formed instead indicating the initial droplets on the surface. Here the surface is locally depassivated and covered by thin corrosion layers, such as iron carbonate or iron hydroxide. Fig. 8 represents the presence of oxygen within the corroded areas of the sample surfaces.

When areas of former droplets consolidate the outer areas corrode the most, resulting in small pits surrounding the former droplet where a multiphase boundary (water, metal, supercritical CO_2) enhances corrosion processes. Consolidation is much more time consuming than the precipitation of small droplets. Therefore more water diffuses back into the supercritical CO_2 and then reduces the area of consolidated droplets towards their centre leaving sulphates ($FeSO_4$) in the outer areas whereas the centre shows hematite (Fe_2O_3). In general, the leopard shaped corrosion layer reveals siderite $FeCO_3$ and goethite a-FeOOH als precipitation phases.

Corrosion rates and local corrosion are decisive when deciding if the steels are suitable for CCS application. Steels will be unsuitable for its use in pressure vessel applications if the corrosion rate exceeds 0,1 mm/year. Furthermore, pitting corrosion is not allowed on specimens' surface to fulfill the regulations of DIN 6601. There is a notable risk of having a notch effect in the surface due to the pitting corrosion. Notches may be the cause of fractures and the following failure of the component. Due to pit growth as a statistical phenomenon with little predictability it cannot be calculated as easily as surface corrosion rates. Therefore reliable corrosion rates and lifetime predictions regarding pit corrosion in CCS technology are not possible.

4. Conclusion

Coupons of the steel quality X5CrNiCuNb16-4 that may be used as injection pipe with 16% Chromium and 0.05% Carbon (1.4542, AISI 630) were exposed up to approximately 1 year (8000 h) to supercritical CO_2 and saline aquifer water at ambient pressure as well as 100 bar and 60 °C in laboratory experiments.

At ambient pressure the least corrosive attack is achieved by a continuous martensitic microstructure. At 100 bar normalizing gives best surface corrosion resistance when the steel is exposed to CO_2-saturated saline aquifer water and hardening + tempering at 670 °C provides good corrosion resistance when the steel is exposed to water saturated supercritical CO_2. At 100 bar the maximum corrosion rate in the liquid phase is approximately 0.014 mm/year, after 8000 h and approximately 0.003 mm/year in the supercritical phase.

Non-uniform corrosion layer ("leopard"-shape) reveal carbonate corrosion products on the surface such as $FeCO_3$ and FeOOH. Within the typical ellipsoids Fe_2O_3 precipitates as a result of changing water solubility in supercritical CO2 due to high pressure.

1.4542 in all states of heat treatments fails the requirements for pressure vessel application according to DIN 6601, because even though the corrosion rates are all tolerable (below 0.1 mm/year), the maximum pit depth exceeds 0.2 mm when the steel is surrounded by the CO_2-saturated brine. Even with low surface corrosion rates, pit growth rates only allow the steel to be suitable for injection pipes in CCS environments if monitored closely.

5. Acknowledgement

This work was supported by the FNK (Fachkonferenz für wissenschaftlichliche Nachwuchskräfte) of the Applied University of Berlin, HTW and by IMPACT (EU-Project EFRE 20072013 2/21).

6. References

[1] Thomas, DC. Carbon Dioxide Capture for Storage in Deep Geologic Formations – Results from CO2 Capture Project, Volume 1: Capture and Separation of Carbon Dioxide form Combustion Sources, CO_2 Capture Project, Elsevier Ltd UK 2005, ISBN 0080445748.

[2] Ruhl, A, Goebel A, Kranzmann A. Corrosion Behavior of Various Steels for Compression, Transport and Injection for Carbon Capture and Storage , Energy Procedia 23 (2012) 216-225

[3] Gale J, Davison J. Transmission of CO_2 – safety and economic considerations, Energy 29 (2004) 1319–1328.

[4] Eldevik F. Graver B, Torbergsen LE, Saugerud OT. Development of a guideline for safe, reliable and cost efficient transmission of CO_2 in pipelines, Greenhouse Gas Control Technologies 9 1 (2009) 1579–1585.

[5] Russick E, Poulter GA, Adkins CLJ. Sorensen NR. Corrosive effects of supercritical carbon dioxide and cosolvents on metals, The Journal of Supercritical Fluids, 9 (1996) 43 50.

[6] Förster A. Norden B. Zinck-Jørgensen K. Frykman P. Kulenkampff J, Spangenberg E, Erzinger J, Zimmer M, Kopp J, Borm G, Juhlin C, Cosma C, Hurter S. Baseline characterization of the CO2SINK geological storage site at Ketzin, Germany: Environmental Geosciences, V. 13, No. 3 (September 2006), pp. 145-161.

[7] Förster A. et al. "Reservoir characterization of a CO2 storage aquifer: The Upper Triassic Stuttgart Formation in the Northeast German Basin," Mar. Pet. Geol. 27, (2010): p. 2156–2172.

[8] Kissinger V. Noack, S. Knopf, D. Scheer, W. Konrad, H. Class, Characterization of reservoir conditions for CO_2 storage using a dimensionless Gravitational Number applied to the North German Basin, Sustainable Energy Technologies and Assessments 7 (2014) 209–220.

[9] Wei L, Pang X, Liu C, Gao K. Formation mechanism and protective property of corrosion product scale on X70 steel under supercritical CO_2 environment, Corrosion Science 100 (2015) 404–420

[10] Nešić S. Key issues related to modelling of internal corrosion of oil and gas pipelines – A review, Corrosion Science 49 (2007) 4308–4338.

[11] Carvalho, DS, Joia CJB, Mattos OR. Corrosion rate of iron and iron-chromium alloys in CO_2-medium, Corrosion Science 47 (2005) 2974-2986.

[12] Cui ZD., Wu SL., Zhu SL., Yang XJ. Study on corrosion properties of pipelines in simulated produced water saturated with supercritical CO_2, Applied Surface Science 252 (2006) 2368-2374.

[13] Pfennig A. Kranzmann A. Reliability of pipe steels with different amounts of C and Cr during onshore carbon dioxid injection, International Journal of Greenhouse Gas Control 5 (2011) 757–769.

[14] Wu SL, Cui ZD, Zhao GX, Yan ML, Zhu SL, Yang XJ. EIS study of the surface film on the surface of carbon steel form supercritical carbon dioxide corrosion", Applied Surface Science 228 (2004) 17-25.

[15] Akbari Mousavi SAA, Sufizadeh AR. Metallurgical investigations of pulsed Nd:YAG laser welding of AISI 321 and AISI 630 stainless steels, Materials & Design 30, Issue 8, (2009) 3150-3157.

[16] Wang J, Zou H. Relationship of microstructure transformation and hardening behavior of type 630 stainless steel. J Univ Sci Tech Beijing 3 (2006) 213–221.

[17] Pfennig H, Wolthusen, Wolf M, Kranzmann A. Effect of heat treatment of injection pipe steels on the reliability of a saline aquifer water CCS-site in the Northern German Basin, Energy Procedia 63 (2014) 5762 – 5772.

[18] Bilmes PD, Llorente CL, Méndez CM, Gervasi CA. Microstructure, heat treatment and pitting corrosion of 13CrNiMo plate and weld metals, Corrosion Science 51 (2009) 876-882.

[19] Bülbül S, Sun Y. Corrosion behaviours of high Cr-Ni cast steels in the HCl solution, Journal of Alloys and Compounds 598 (2010) 143-147.

[20] Cvijović Z. and Radenković G. Microstructure and pitting corrosion resistance of annealed duplex stainless steel, Corrosion Science 48 (2006) 3887-3906.

[21] Hou Y, Li J, Zhang, Effect of alloy elements on the anti-corrosion properties of low alloy steel, Bull. Mater. Sci. 23 (2000) 189-192.

[22] Zhang L, Zhang W, Jiang Y, Deng B, Sun D, Li J. Influence of annealing treatment on the corrosion resistance of lean duplex stainless steel 2101, Electrochimica Acta 54 (2009) 5387–5392.

[23] Choi Y-S, Kim J-G, Park Y-S, Park J-Y. Austenitzing treatment influence on the electrochemical corrosion behaviour of 0.3C-14Cr-3Mo martnesitic stainless steel, Materials Letters 61 (2007) 244-247

[24] Isfahany AN, Saghafian H, Borhani G. The effect of heat treatment on mechanical properties and corrosion behaviour of AISI420 martensitic stainless steel, Journal of Alloys and Compounds 509 (2011) 3931-3936

[25] Park J-Y, Park Y-S. The effects of heat-treatment parameters on corrosion resistance and phase transformation of 14Cr-3Mo martensitic stainless steel, Materials Science and Engineering A 449-451 (2007) 1131-1134

[26] Dyja Z, Stradomski A. Pirek. Microstructural and fracture analysis of aged cast duplex steel, Strength of Materials, Vol. 40, No. 1 (2008) 122-125

[27] Lucio-Garcia MA, Gonzalez-Rodrigueza JG, Casalesc M, Martinezc L, Chacon-Navaa JG, Neri-Floresa MA and Martinez-Villafañea A. Effect of heat treatment on H_2S corrosion of a micro-alloyed C–Mn steel, Corrosion Science 51 (2009) 2380-2386

[28] Banaś J, Lelek-Borkowska U, Mazurkiewicz B, Solarski W. Effect of CO_2 and H_2S on the composition and stability of passive film on iron alloy in geothermal water, Electrochimica Acta 52 (2007) 5704-5714.

[29] Moreira RM, Franco CV, Joia CJBM, Giordan S, Mattos OR. The effects of temperature and hydrodynamics on the CO_2 corrosion of 13Cr and 13Cr5Ni2Mo stainless steels in the presence of free acetic acid, Corrosion Science 46 (2004) 2987-3003.
[30] Seiersten M, Material selection for separation, transportation and disposal of CO_2, Corrosion paper no. 01042 (2001).
[31] Choi Y-Y and Nešić S. Determining the corrosive potential of CO_2 transport pipline in high pCO_2-water environments, Journal of Green House Gas Control 5 (2011) 788-797.
[32] Han J, Zhang J, Carey JW, Effect of bicarbonate on corrosion of carbon steel in CO_2-saturated brines, Journal of Green House Gas Control 5 (2011) 1680-1683.
[33] Pfennig A, Kranzmann A. 2012, Effect of CO2 and pressure on the stability of steels with different amounts of Chromium in saline water, Corrosion Science 6 (2012) 441–452
[34] Pfennig A, Linke B, Kranzmann A, Corrosion behavior of pipe steels ex-posed for 2 years to CO_2-saturated saline aquifer environment similar to the CCS-site Ketzin, Germany, Energy Procedia, Vol. 4 (2011) 5122-5129.
[35] Mu LJ, Zhao WZ. Investigation on carbon dioxide corrosion behavior of HP13Cr110 stainless steel in simulated stratum water, Corrosion Science 52 (2010) 82-89.
[36] Pfennig A, Heynert K, Wolf M, Böllinghaus T. First in-situ Electrochemical Measurement During Fatigue Testing of Injection Pipe Steels to Determine the Reliability of a Saline Aquifer Water CCS-site in the Northern German BasinOriginal, Energy Procedia, 63 (2014) 5773-5786.
[37] Pfennig A, Zastrow P, Kranzmann A. Influence of heat treatment on the corrosion behaviour of stainless steels during CO_2-sequestration into saline aquifer, International Journal of Green House Gas Control 15 (2013) 213–224.